Linear ripples and traveling circular ripples produced on polymers by thermal AFM probes

Enrico Gnecco,[1,*,†] Elisa Riedo,[2] William P. King,[3] Seth R. Marder,[4] and Robert Szoszkiewicz[5,*,‡]
[1]*Department of Physics, University of Basel, Klingelbergstrasse 82, 4056 Basel, Switzerland*
[2]*School of Physics, Georgia Institute of Technology, Atlanta, Georgia 30332, USA*
[3]*Department of Mechanical Science and Engineering, University of Illinois Urbana–Champaign, Urbana, Illinois 61801, USA*
[4]*School of Chemistry and Biochemistry, Georgia Institute of Technology, Atlanta, Georgia 30332, USA*
[5]*Department of Physics, Kansas State University, Manhattan, Kansas 66506, USA*
(Received 19 February 2009; revised manuscript received 8 May 2009; published 18 June 2009)

We discuss the time and temperature evolution of the nanometer-scale surface undulations (ripples) produced by a heated atomic force microscope (AFM) tip scanning across surfaces of several amorphous polymers. During linear zigzag scanning we obtain pseudolinear ripples approximately perpendicular to the fast scan direction in a range of scan rates and probe temperatures. As expected, the size of the ripples increases massively in the vicinity of the glass temperature for each polymer. We also examine a different case in which the AFM tip follows a circular path. Contrary to the "steady" linear ripples we obtain circular ripples which rotate along the scanning path during consecutive scans. The group velocity of the circular ripples is 2 orders of magnitude lower than the scan speed. We interpret the experimental data using a phenomenological model accounting for erosion and smoothing effects caused by the probing tip.

DOI: 10.1103/PhysRevB.79.235421 PACS number(s): 81.16.Nd, 82.35.Gh, 07.79.Lh, 45.70.Qj

I. INTRODUCTION

The formation of ripple patterns on fragile surfaces subject to external perturbations occurs commonly over a range of length scales. Macroscopic linear ripples with wavelengths between several centimeters and several meters are often created by wind on sandy deserts and sea shores.[1,2] These ripples arise from interactions of high-energy long-leaping sand grains with the low-energy short-leaping grains. Similar to sand ripples, ion sputtering experiments on metal substrates (such as argon sputtering on Ag) have produced microripples with wavelengths ranging between tens of nanometers to submicrometers.[3] It has been shown that the properties of the incident ion beam and the properties of the bombarded surface lattice determine the shape and orientation of these microripples. Finally, nanoripples with wavelengths between several tens of nanometers and hundreds of nanometers have been obtained by scanning a substrate with an atomic force microscope (AFM) tip. Nanoripples have been observed after many subsequent zigzag scans over the same micrometer-size areas of polymers,[4–9] ionic salts,[10] metals,[11] and semiconductors.[12] Nanoscale ripples on polymers have been produced in just one AFM scan using either a heated polymer surface[13] or a heated AFM probe.[14,15] These ripples are approximately linearly shaped and align normal to the AFM fast scanning direction.

The evolution of sand macroripples and ion-sputtered microripples is usually described by complicated fourth-order differential equations, which take into account competitive processes of surface erosion and relaxation.[16,17] In contrast, nanoripples produced by repetitive localized scanning have only been interpreted using simplified and qualitative models. In the case of polymers, these models relate the evolution of ripples to polymer properties alone,[9,18] local cracks formation and subsequent polymer peeling,[19] or minuscule wearing off the surface during each scan.[20] Even less is known for nanoripples produced on polymers using heat. Clearly, the heat changes compressive and tensile stresses in a substrate due to poking it with an AFM tip but a quantitative interpretation is still elusive. Furthermore, the experiments and models have been limited to linear ripples; however, an enhanced repertoire of ripple geometries, such as circular ripples, could lead to more diverse applications, e.g., templates[21] for custom nanosorting or nanoassembly and structures for nanoplasmonics and nanoptics.[22–26]

Here, we investigate the ripples created on several polymer films by a resistively heated AFM probe under a range of scanning conditions. We start by establishing a firm connection to the previously published results. Thus, we produce the pseudolinear ripples at several heating conditions and scanning speeds. We find massive enhancement of linear ripple wavelengths in proximity of the glass temperature, which is consistent with previous investigations. Next, we investigate a case in which a heated AFM probe follows a circular path rather than a typical zigzag path. Circular scanning produces circular ripples aligned along the scanned pathway. Circular ripples tend to rotate along the scan direction and thus are far more dynamic than pseudolinear ripples. We measure their group velocity and we reproduce their evolution in silico by introducing a phenomenological model based on interplay between surface erosion and surface relaxation.

II. EXPERIMENTAL

In our AFM experiments we used resistively heated probes (rh levers) (Refs. 27–29) in the contact mode with different polymer samples: a poly(methylmethacrylate) (PMMA, $M_w \sim 120$ kD), a polycarbonate (PC, $M_w \sim 20-25$ kD), and a polysulfone (PSul, $M_w \sim 44-53$ kD). Polymer powders (Sigma-Aldrich, USA) were dissolved in toluene and spin coated on a nanorough glass substrate (Fisher Scientific, USA) to yield ~ 1-μm-thick polymer films. The rh levers were custom mounted in a Multimode

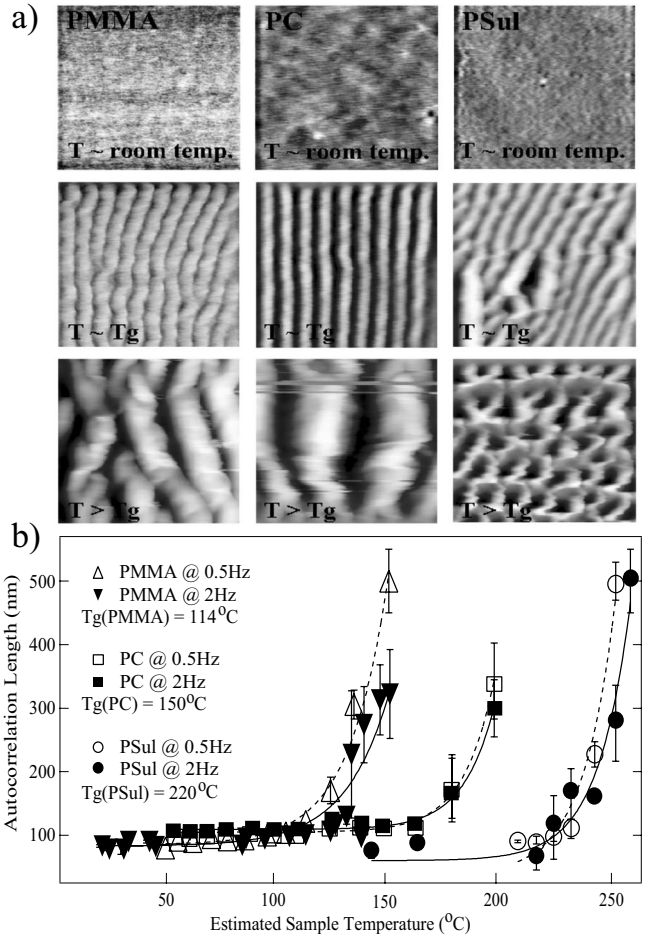

FIG. 1. (a) 1×1 μm^2 AFM contact-mode images of ripples created by rastering polymer films (spin coated on glass substrates) with a resistively heated AFM probe at several temperatures. (b) A plot of the autocorrelation lengths obtained from (a) reveals an exponential growth of the ripple wavelengths with temperature. Data obtained for 0.5 Hz (fitted with broken lines) and for 2 Hz (fitted with solid lines) scanning speeds are presented for each polymer.

IVa AFM (Veeco, USA) designed for a zigzag surface scanning and equipped with a homemade module for a circular surface scanning. Our AFM uses a standard laser-beam bounce-detection scheme for sensing the cantilever deflection.

We obtained a tip-polymer temperature profile based on the thermal calibration of the rh levers[28] and a finite-element steady-state solution of the heat-transfer equation from a cantilever to a polymer surface.[30] We supposed that heat transfer from the rh lever to the polymer surface occurs mostly by conduction through a tip from an area just above the tip.[28] We used typical thermal properties of the polymers as well as typical dimensions and thermal properties of the rh levers.[15,28,31]

III. RESULTS AND DISCUSSION

A. Linear ripples

Figure 1(a) shows a few examples of 1×1 μm^2 AFM images of pseudolinear ripples obtained (i) at room temperature, (ii) in the vicinity of the glass transition temperature, T_g, and (iii) above T_g. A flat polymer surface is modified during one AFM scan giving rise to a very regular pattern when the local surface temperature is close to the characteristic T_g of the polymer. Once the surface temperature is greater than T_g the patterns can be chaotic and the quasilinear arrangements of the ripples is often lost. By autocorrelating each of the AFM images, we find the characteristic wavelength of the ripples, λ, for each investigated temperature and scanning speed. In Fig. 1(b) we plot the obtained autocorrelation lengths versus estimated local temperature for each substrate. Below T_g the corresponding λ remains in the order of 100 nm for each polymer. Above T_g the value of λ increases abruptly in an exponential-like fashion.

The sudden increase in the wavelength λ beyond the glass transition temperature T_g has already been reported and used to estimate the value of T_g for some polymer samples.[14,32,33] Similar to our results, Ref. 13 reported $\lambda\sim100$ nm below the polymer T_g while repetitively scanning preheated polystyrene films with regular AFM cantilevers. However, the ripples obtained by repetitive scanning grew linearly with temperature at $T\geq T_g$, which is in contrast to the exponential increase we observe. We qualitatively explain our data and this controversy using continuum contact mechanics.[34,35]

The critical normal force, F_c, exerted by a stiff AFM tip at the tip-polymer contact and at the onset of plastic deformation, is proportional to the plastic yield stress, σ_c, and the contact area, A_r: $F_c=\sigma_c A_r$. Due to the extensive compliance of polymers, the value of A_r is essentially determined by the tip profile and thus related to the ripple wavelength, λ. Describing the tip as a cone with an opening angle α, we estimate $\lambda\sim2(\delta\tan\alpha+R)$; here δ is the indentation depth and R is the AFM tip curvature radius. We have supposed that (i) on the sides of an indent δ the polymer adjusts to the tip shape $\delta\tan\alpha$ since polymer is soft and the tip can penetrate deeply and (ii) the edges of an indent are shaped correspondingly to the tip radius R since the tip will move around them back and forth in the zigzag scans. The tip is symmetric so it comes as a factor of 2. Due to large indentation depths we neglect the tip-sample adhesion energy and $\delta\sim A_r/R$.[34,35] Furthermore, we assume elastic-plastic contact area boundary and obtain a final estimate: $\lambda\sim2[3.2F_c\tan\alpha/(\sigma_c R)+R]$.

Phenomenologically, it has been shown that for unoriented macroscopic polymer films the value of σ_c decreases linearly with temperature up to the glass transition temperature, and past T_g, the value of σ_c starts to decrease exponentially with temperature.[36] Assuming that $\alpha=30°$, $R=20$ nm, $F_c=30$ nN, and $\sigma_c=1$ GPa (typical for many unoriented polymers such as PS or PMMA), we get $\lambda\sim50$ nm at room temperature. Just above the glass transition temperature σ_c has been reported to drop by 50–90 %,[36] which yields much larger values of λ (consistent with our data). Furthermore, at the macroscopic scale Ref. 36 reported that σ_c is linearly dependent on the temperature above T_g if the polymer has been prestretched. This is likely the case reported in Ref. 13, where the sample was scanned many times and globally heated.

Figure 1(b) shows that a slower scanning speed produces a faster rate of λ increase with temperature. Solutions of

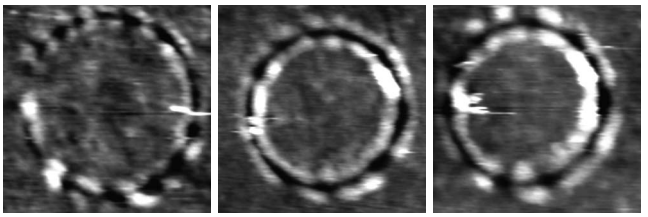

FIG. 2. AFM images (contact mode, topography signal) of three different circular ripples created by a resistively heated AFM tip. An image on the left is 410×410 nm^2, in the middle is 445×445 nm^2, and on the right 375×375 nm^2. All images have been obtained after only a few circular scans with a hot rh tip. Peak to valley distances are around several nm.

heat-transfer equations for our rh levers show that the steady state, and thus, stabilization of the temperature at the tip-sample interface, is reached within several microseconds.[15] Thus, there is enough time to reach thermal equilibrium in each one of the 256 AFM data points acquired at 0.5 and 2 Hz scan rates for each scan pass. A faster increase in the autocorrelation length at a lower scanning speed displays some relations to the time-dependent viscoelastic and plastic deformations of the polymer surface.[13]

B. Circular ripples

Having examined the linear ripples, we proceeded to scratch a polymer surface in a circular way. Figure 2 shows a few contact-mode AFM images taken after several consecutive circular scans of the PMMA sample with a tip heated in vicinity of the corresponding T_g. The ripples created within a circumference of the scanned circles are clearly distinguishable.

To investigate *in situ* formation of circular ripples in greater detail, we have recorded instantaneous variations in the vertical displacement of the cantilever while scanning a PMMA surface with only minimal AFM feedback. We investigated several temperatures and two different scanning speeds. After binomial smoothing (Igor Pro, Wavemetrics, USA), the recorded cantilever displacement follows a pseudosinusoidal function with visible undulations (Fig. 3). These bumpy undulations correspond to major ripples, while the pseudosinusoidal background reflects the cantilever buckling while forced to follow a circular path instead of a linear zigzag path.

We can trace the position of individual ripples during consecutive scans. By following the same maxima (or minima) over many scanning cycles, it appears evident that the ripples can move during consecutive scans in a similar manner as a wave packet travels in space, and thus, we can calculate their corresponding group velocity. Figure 4 shows the position of all the detected maxima in each period vs time. For each maximum, the position is measured with respect to the same arbitrary circular angle. When the ripple position overcomes 360°, the ripple reappears at 0° similar to the case of periodic boundary conditions.

While scanning with a nonheated cantilever [Fig. 4(a)] we have initially noticed an irregular progression of the ripples. However, after several cycles (around $t>40$ s), a few given

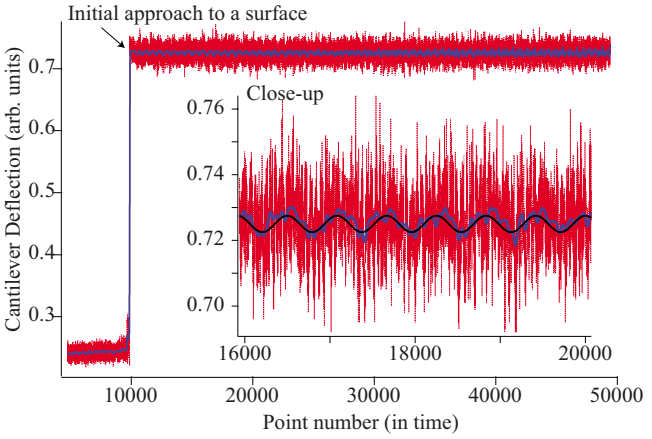

FIG. 3. (Color online) The formation/migration kinetics of circular ripples is obtained from direct acquisition of a cantilever deflection signal while rastering a heated AFM probe in a circular fashion. To localize the onset of ripple formation we start to record the cantilever deflection (most oscillating curve, red online) ahead of a tip-polymer first contact. Superimposed on the raw deflection data are smoothed deflection data (blue online, binomial smoothing, Igor Pro, Wavemetrics, USA). An undulated quasisin wave function appears after smoothing the deflection data, as depicted on the closeup of the initial portion of the deflection data (figure inset). A fitted sinusoidal wave function is showed in black as well. Undulations correspond to the most pronounced ripples (protrusions) created/moved during each period of tip scanning.

ripples begin to be collectively displaced. The circumference of a scanned circle was 1.1 ± 0.1 μm and the scanning rate was 0.51 ± 0.01 Hz. By calculating the slopes of the curves in Fig. 4(a), we obtain group velocities ranging between 5 and 8 nm/s, i.e., up to 0.015 times the cantilever scanning velocity.

In Fig. 4(b) we increased the temperature at the cantilever—sample interface (by heating rh levers) to $45\ ^\circ\mathrm{C}\pm15\ ^\circ\mathrm{C}$ (still below the T_g of PMMA, i.e., about 115 °C). We observed that several ripples moved with group velocities between 5 and 8 nm/s. Figures 4(c) and 4(d) were obtained at different positions on the sample but still at the tip-sample interface temperature of $45\ ^\circ\mathrm{C}\pm15\ ^\circ\mathrm{C}$. Initially, the ripples travel with typical velocities between 5 and 13 nm/s (or 0.024 times the cantilever speed). After some cycles (about 20–30 scans) they slow down, e.g., to velocities <0.5 nm/s on Fig. 4(d).

We discuss the decrease in group velocity in the next section (based on our model). Here we mention, however, that such a decrease with time might also be affected by drift. We associate vertical or, respectively, lateral drifts with all the time-dependent processes (such as cantilever, sample, and AFM piezo creeps), which change the normal force (load) or, respectively, provoke departures from circular scanning. Along with the vertical cantilever position change (presented in Fig. 4) we have recorded (not presented here) the friction signal between the sample and the tip (the so-called "LFM" or lateral force microscopy signal). The friction signal scales with the normal force. Thus, at a given load, the mean friction signal (averaged over a period of circular ripples) is a good indicator of vertical drift. For the

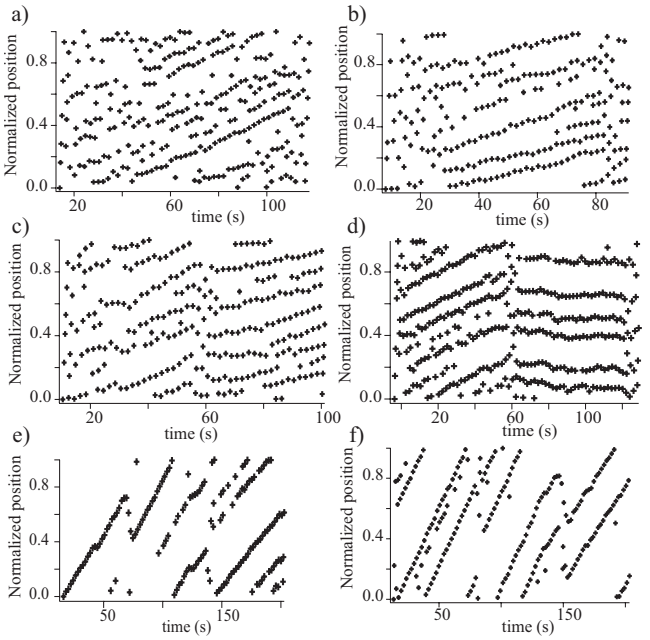

FIG. 4. Following the maxima (or minima) of the undulations, superimposed to a quasisin wave function in Fig. 3 during each circular scan, provides for the migratory pattern of circular ripples. Here, we detect maxima within the undulations and plot their normalized position (within a circular period) vs time. (a)–(d) correspond to 0.56 ± 0.05 μm/s AFM tip velocity and (a) room or (b)–(d) 45 ± 15 °C tip-sample interface temperature; (e)–(f) are obtained with 5.6 ± 0.5 μm/s AFM tip velocity and for (e) 125 ± 20 °C or (f) 175 ± 20 °C tip-sample interface temperature.

data reported in this paper, we have not observed any change in a mean friction over the measurement times. Furthermore, careful analysis of AFM topographs presented in Fig. 2 shows that the measured width of the ripples is within the approximated value for the elastic-plastic indentations at our experimental conditions. Thus, any lateral drift is likely below our detection limit.

Finally, Figs. 4(e) and 4(f) show traveling circular ripples at temperatures around and above the PMMA T_g and at a 10× larger scanning speed (10× larger circumference, the same period) than before. In Fig. 4(e) the tip-sample temperature has been calculated to be 125 °C ± 20 °C, which is around the PMMA T_g. The mean group velocity of these ripples ranges between 120 and 190 nm/s, i.e., 0.020–0.034 times the cantilever speed. In Fig. 4(f) the tip-sample temperature is 175 °C ± 20 °C and the group velocity of the circular ripples ranges between 150 and 200 nm/s, i.e., between 0.026 and 0.036 times the cantilever speed. In both cases, the group velocities slow down with time.

Our results show that the circular ripples are created and moved collectively in a range of group velocities, which (i) are 2 orders of magnitude slower than the tip scanning speed and (ii) can decrease with time. These group velocities, however, increase with the temperature of the tip-sample interface as well as with the scanning speed. Curiously, group velocities around and above T_g [Figs. 4(e) and 4(f)] are comparable to the typical migration speeds of sand dunes, such as sand dunes in Leba, Poland moving at 3 m/yr, e.g., about 100 nm/s.

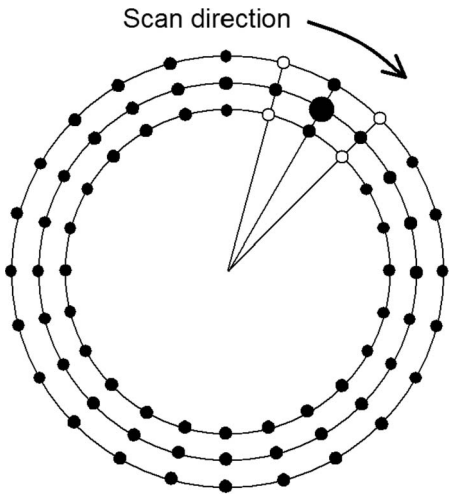

FIG. 5. The scan path used to form ripples (intermediate circle) together with two concentric auxiliary circles. The big black dot represents the location where the process described in the text occurs. This dot is surrounded by four first neighbors and four second neighbors (empty dots represent the latter).

C. Phenomenological interpretation

We start to discuss our results with the case of the circular ripples. We consider a circle of radius R lying on a flat area and select L points, equally spaced along the circle, as well as $2L$ side points on two concentric "auxiliary" circles, as shown in Fig. 5. The first circle is then repeatedly scanned clockwise (N times) by an ideal tip. While scanning, the tip modifies the surface, which is much softer than the tip itself. In our model, we assume that the evolution of the surface topography depends on its slope along the scan path. Due to directionality of the tip motion, we assume that the profile grows in the presence of a negative slope, decreases with positive slope, and remains unchanged for a flat surface.

The profile evolution is parametrized as follows. At each of the L points, the height, z, can (i) decrease by a fixed value H (in the units of height u_z) with a probability p_- and (ii) increase by H with another probability p_+. The quantities $p_\mp$ depend on the local slope z', according to the formulas

$$p_\mp = \frac{1 \pm \tanh(2z')}{2}. \tag{1}$$

The values p_- and p_+ are between 0 and 1, and the slope z' is simply estimated by the height increase between the selected location and the next first neighbor in the scan direction. When the profile is flat $p_-=p_+$ whereas $p_->p_+$ (or $p_-<p_+$) when the slope z' is positive (or negative). The parameter H can be interpreted as the erosion rate of the surface scratched by the tip.

The variation in the height z is immediately compensated by a smoothening process similar to the one described in Ref. 20. The height $z(\bullet)$ of the site $(\bullet)$ is increased by the quantity

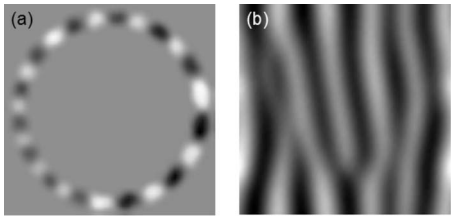

FIG. 6. (a) Circular ripples produced by 1000 scans on 150 points aligned on a circle. This image has been smoothened to reduce discretization effects. (b) Pseudolinear ripples produced by 1000 zigzag scans on a square lattice of 70×70 points. In both cases, the surface relaxation occurs with a coefficient $D=0.5$.

$$\Delta z = D\left(\sum_{1\text{st}} \frac{z}{6} + \sum_{2\text{nd}} \frac{z}{12} - z(\bullet)\right)u_z,$$

where D is a surface relaxation coefficient and the sums are extended to the first and second neighbors of the selected location (●), defined as in Fig. 5. At the same time, the heights at the first and second neighbors are decreased in the quantities $\Delta z/6$ and $\Delta z/12$, respectively. The values 6 and 12 are chosen to keep the total "mass" of the polymer constant and to enhance the smoothening effect at the first neighbors compared to the second ones. Thus, a small bump (or depression) is created when the tip moves downward (or, respectively, upward). The height or depth of these features is determined by the erosion and relaxation coefficients H and D and by the local topography.

Under these assumptions, however, the amplitude of the scanned profile would increase without limits. This nonphysical result can be prevented by assuming that the curvature of the profile cannot exceed the tip curvature R^{-1}. For this reason, we estimate the second derivative z'' of the surface profile along the scan direction and impose the constraint $|z''|<R^{-1}$ in our calculations. More precisely, we could have assumed $|z''/(1+z')^{3/2}|<R^{-1}$ but it does not change our qualitative conclusions. We obtain consistency with other results (see below) assuming that $|z''|_{\max}=50u_z/u_t^2$, where u_t is the length unit along the circumference.

Figure 6(a) shows the results of a simulation corresponding to $D=0.5$, $H=10$, $L=150$, and $N=1000$. A pattern of 13 circular ripples is formed. For comparison, a pattern of pseudolinear ripples produced with a similar mechanism on a square lattice of 70×70 points after $N=1000$ zigzag scans is shown in Fig. 6(b). The corrugation (amplitude) of the circular pattern increases almost linearly with time until the maximum value $|z''|_{\max}$ is reached at some locations. At this point, the amplitude starts to fluctuate around a given saturation value (for our choice of parameters: $z_{\text{sat}}\sim500u_z$).

The evolution of the circular ripple profile with time is shown in Fig. 7 and it shares many qualitative similarities to our experimental results (Figs. 2 and 4). First, the number of ripples, and consequently the average "wavelength" of the profile, does not change with time. Second, the ripple pattern tends to rotate along the scan direction during consecutive scans. Third, the group velocity of the ripples slows down with time.

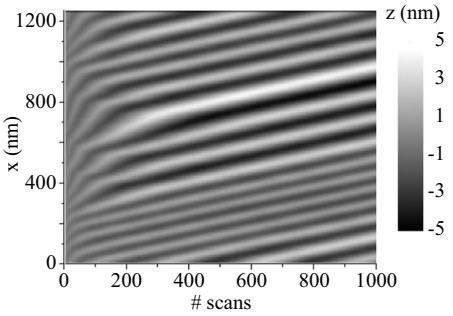

FIG. 7. Time evolution of the ripple profile [height changes in a path, x (nm), along the scanned circle vs scan number]. With the parameters used in Fig. 6 the group velocity slows down from 1.5 to 0.15 nm/s.

In order to compare our model quantitatively to the experimental results, we need to "calibrate" the length units u_z and u_t. Their order of magnitude is given by a comparison with the radius of the circle scanned in the AFM experiment and the saturation value of the ripple amplitude. Assuming that the scanned circle has a radius of 200 nm and the ripple corrugation is about 10 nm, as in the experiments, we estimate that the distance u_t between consecutive points in Fig. 5 is about 10 nm and the height unit u_z in our simulations is approximately 0.02 nm. With these values, the maximum value for the ripple curvature becomes $|z''|_{\max}=50u_z/u_t^2=0.01$ nm^{-1}. This value corresponds to a tip radius in the order of 100 nm, which is consistent with the experimental results. Assuming a scan rate of 0.5 Hz, similar to the experiments, the speed of rotation of the ripples, as estimated from Fig. 7, takes the value of 1.5 nm/s in the first scans and then it decreases to 0.15 nm/s after about 100 scans. This theoretical group velocities for the above chosen values of H and D compare quite well with the experimental results obtained around room temperature. There, the group velocity initially ranged between 5 and 13 nm/s and after 20–30 scans slowed down significantly, e.g., to <0.5 nm/s in Fig. 4(d). However, quantitative agreement is only approximative, above all at a higher temperature where the experiments show group velocities around 200 nm/s.

This leads us to discuss the assumptions of our model more thoroughly. First, the parametrization of an initial indentation and erosion zone can be the source of discrepancy between the experimental and theoretical results. The high compliance of the polymers, particularly at elevated tip-sample temperature, results in a much larger contact area than on a hard surface. Enhanced erosion area in our model corresponds to lower number of points within the circle and results in larger group velocities. Second, the number of points associated with the area where the relaxation process occurs introduces noticeable discretization in the simulations. Increasing the density of these points would require an accurate parametrization of the tip shape which is beyond the scope of our phenomenological model. Next, any form-factor variation in the functions $p_{\pm}$ [Eq. (1)] essentially renormalizes the values of H and D. Thus, we conclude by discussing how H (characterizing rate of erosion) and D (characterizing the surface relaxation coefficient) contribute to the formation of circular ripples. Circular ripples are observed only in a

certain range of the parameters D and H. If D is too small, only scattered localized wave packets appear. Instead, if D increases beyond a certain value, we observe that exceptionally large peaks tend to emerge from the ripple pattern and to quickly propagate and destroy the ordering of the ripple structure. The higher is H, the smaller is the number of ripples that are formed. These conclusions are consistent with simulations of patterns formed on sand and ion-sputtered surfaces, which predict the ripple formation only in a certain range of the parameter values used to describe erosion and relaxation at the surfaces.[17] Finally, the values of H and D currently depend on the tip temperature in an unknown way. The values of D and H chosen in Fig. 6 are in the region where regular ripple evolution is observed but they should not be interpreted too strictly without a conspicuous amount of experimental results under different scan conditions. Only a massive amount of experimental data along with further analytical insight is expected to unfold discussed above dependencies and to produce more viable quantitative comparisons between experimental and theoretical group velocities of traveling ripples.

IV. CONCLUSIONS

We have investigated the formation of linear and circular ripples obtained by scanning several polymer surfaces with heated AFM probes. First, the polymers, i.e., PC, PMMA, and PSul, have been locally zigzag scanned in a range of tip-surface temperatures from room temperature to above the glass transition temperature for each sample. Thermal properties of the tip and the polymer samples have been used for temperature calibration. The obtained linear ripples have showed periodicity, i.e., wavelengths, λ, between about 100 nm at room temperature up to several hundreds of nanometers above T_g. The wavelength λ increases linearly and slowly with T below T_g and in a exponential-like fashion above T_g. Such temperature dependence has been qualitatively explained taking into account the mechanical properties of the tip-sample contact as well as the macroscopic dependence of the polymer mechanical properties, namely, the shear strength with temperature.

By *in situ* circular scanning on the PMMA surface using a heated thermal probe, we have obtained traveling circular ripples. We have calculated their collective traveling speed, i.e., group velocity, as ranging between a few to tens of nanometers per second and depending on the scanning rate and the tip-surface temperature. Both an increase in the scanning speed and the temperature have resulted in larger group velocities. We have adopted a phenomenological model to simulate the circular ripples. Our model is based on the surface erosion, depending mostly on the local slope of the ripple profile, as well as the surface relaxation, depending chiefly on the tip pressure. Qualitatively, the model reproduces the ripple rotation. Both experiments and model agree that the ripples rotate within a certain range of group velocities and that the rotation speed decreases with time. Depending on the tip-surface temperature, the group velocity predicted by the model is up to 2 orders of magnitude slower than that one obtained in the experiments. Thus, further analytical work and experimental results are necessary to relate the group velocity to the temperature-dependent erosion and relaxation rate of the polymer surface under the pressure of a sliding tip.

ACKNOWLEDGMENTS

The authors acknowledge financial support from the Department of Energy under Grant No. DE-FG02-06ER46293 and the Swiss National Center of Competence in Research on Nanoscale Science, and the NSF under Grant No. DMR-0120967.

*Corresponding author.
†enrico.gnecco@unibas.ch
‡rs@phys.ksu.edu

[1] R. Bagnold, *The Physics of Blown Sand and Desert Dunes* (Methuen, London, 1941).
[2] B. Andreotti, P. Claudin, and O. Pouliquen, Phys. Rev. Lett. **96**, 028001 (2006).
[3] U. Valbusa, C. Boragno, and F. B. de Mongeot, J. Phys.: Condens. Matter **14**, 8153 (2002).
[4] O. Leung and M. Goh, Science **255**, 64 (1992).
[5] T. Aoike, T. Yamamoto, H. Uehara, T. Yamanobe, and T. Komoto, Langmuir **17**, 5688 (2001).
[6] R. H. Schmidt, G. Haugstad, and W. L. Gladfelter, Langmuir **19**, 898 (2003).
[7] F. Dinelli, G. J. Leggett, and P. H. Shipway, Nanotechnology **16**, 675 (2005).
[8] M. Surtchev, N. R. de Souza, and B. Jerome, Nanotechnology **16**, 1213 (2005).
[9] G. F. Meyers, B. M. DeKoven, and J. T. Seitz, Langmuir **8**, 2330 (1992).
[10] A. Socoliuc, E. Gnecco, R. Bennewitz, and E. Meyer, Phys. Rev. B **68**, 115416 (2003).
[11] M. Andersson, A. Iline, F. Stietz, and F. Traeger, Appl. Phys. A: Mater. Sci. Process. **68**, 609 (1999).
[12] B. Such, F. Krok, and M. Szymonski, Appl. Surf. Sci. **254**, 5431 (2008).
[13] R. H. Schmidt, G. Haugstad, and W. L. Gladfelter, Langmuir **19**, 10390 (2003).
[14] B. Gotsmann and U. Dürig, Langmuir **20**, 1495 (2004).
[15] R. Szoszkiewicz, T. Okada, S. C. Jones, T.-D. Li, W. P. King, S. R. Marder, and E. Riedo, Nano Lett. **7**, 1064 (2007).
[16] J. Munoz-Garcia, M. Castro, and R. Cuerno, Phys. Rev. Lett. **96**, 086101 (2006).
[17] T. Aste and U. Valbusa, New J. Phys. **7**, 122 (2005).
[18] D. D. Woodland and W. N. Unertl, Wear **203-204**, 685 (1997).
[19] Z. Elkaakour, J. P. Aimé, T. Bouhacina, C. Odin, and T. Masuda, Phys. Rev. Lett. **73**, 3231 (1994).
[20] H. Nishimori and N. Ouchi, Phys. Rev. Lett. **71**, 197 (1993).
[21] E. Mele, F. Di Benedetto, R. Cingolani, D. Pisignano, A. Toma, F. Buatier de Mongeot, R. Buzio, C. Boragno, G. Firpo, V.

Mussi, and U. Valbusa, Nanotechnology **16**, 2714 (2005).
[22] A. M. Armani, A. Srinivasan, and K. J. Vahala, Nano Lett. **7**, 1823 (2007).
[23] A. M. Armani, R. P. Kulkarni, S. E. Fraser, R. C. Flagan, and K. J. Vahala, Science **317**, 783 (2007).
[24] F. Lopez-Tejeira, S. G. Rodrigo, L. Martin-Moreno, F. J. Garcia-Vidal, E. Devaux, T. W. Ebbesen, J. R. Krenn, I. P. Radko, S. I. Bozhevolnyi, M. U. Gonzalez, J. C. Weeber, and A. Dereux, Nat. Phys. **3**, 324 (2007).
[25] C. K. Chang, D. Z. Lin, Y. C. Chang, M. W. Lin, J. T. Yeh, J. M. Liu, C. S. Yeh, and C. K. Lee, Opt. Express **15**, 15029 (2007).
[26] N. Bonod, E. Popov, D. Gérard, J. Wenger, and H. Rigneault, Opt. Express **16**, 2276 (2008).
[27] H. J. Mamin and D. Rugar, Appl. Phys. Lett. **61**, 1003 (1992).
[28] J. Lee, T. Beechem, T. L. Wright, B. A. Nelson, S. Graham, and W. P. King, J. Microelectromech. Syst. **15**, 1644 (2006).
[29] D. Wang, M. Lucas, R. Szoszkiewicz, E. Riedo, T. Okada, S. C. Jones, S. R. Marder, J. Lee, and W. P. King, Appl. Phys. Lett. **91**, 243104 (2007).
[30] W. P. King and K. E. Goodson, ASME J. Heat Transfer **129**, 1600 (2007).
[31] E. A. Grulke, A. Abe, and D. R. Bloch, *Polymer Handbook* (Wiley, New York, 2003).
[32] B. Gotsmann, U. Duerig, S. Sills, J. Frommer, and C. J. Hawker, Nano Lett. **6**, 296 (2006).
[33] S. Sills, H. Fong, C. Buenviaje, M. Sarikaya, and R. M. Overney, J. Appl. Phys. **98**, 014302 (2005).
[34] *Springer Handbook of Nanotechnology*, edited by B. Bhushan (Springer-Verlag, Heidelberg, 2004).
[35] R. Szoszkiewicz, B. Bhushan, B. D. Huey, A. J. Kulik, and G. Gremaud, J. Chem. Phys. **122**, 144708 (2005).
[36] V. I. Vettegren, V. B. Kulik, and S. V. Bronnikov, Tech. Phys. Lett. **31**, 969 (2005).